

DFT Calculations of InP Quantum Dots: Model Chemistries, Surface Passivation, and Open-Shell Singlet Ground States

Preston T. Snee*



Cite This: *J. Phys. Chem. C* 2021, 125, 11765–11772



Read Online

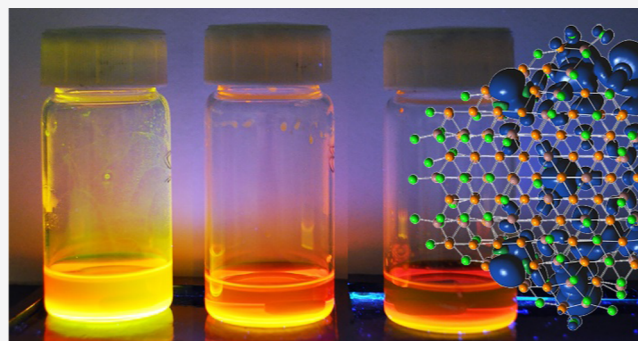
ACCESS |

Metrics & More

Article Recommendations

Supporting Information

ABSTRACT: Density functional theory (DFT) calculations on large clusters of indium phosphide are presented. Several quantum dot-sized models, $(\text{NH}_3)_{64}(\text{InP})_{117}$, $(\text{COOH}_2)_{45}(\text{InP})_{117}$, $(\text{InCl}_3)_{29}(\text{InP})_{147}$, and $(\text{ZnCl}_2)_{29}(\text{InP})_{147}$, were passivated with organic or inorganic ligands; in some systems, both types were used. Initial results with the PBE1PBE functional proved puzzling as many clusters were initially found to have open-shell paramagnetic ground states, which is not sensible for nanoparticles of a direct band-gap semiconductor. In the case of QDs passivated with organic ligands, implementation of a robust geometry optimization procedure demonstrated that these findings were due to localization to metastable states and that the ground states are in fact diamagnetic singlets. However, the “nonstoichiometric” inorganic-passivated clusters $(\text{InCl}_3)_{29}(\text{InP})_{147}$ and $(\text{ZnCl}_2)_{29}(\text{InP})_{147}$ have ground nonet and septet states, respectively. Examination of the molecular orbitals revealed non-Aufbau state filling, suggesting the potential for open-shell singlet ground states, which is supported by calculations at the more robust M06-2x level of theory. Experimental evidence for paramagnetic or open-shell singlet ground states was not realized, which may be due to a mixture of inorganic and organic passivations.



INTRODUCTION

Semiconductor quantum dots (QDs) are nanoparticles that have size-tunable optoelectronic properties through the effects of quantum confinement. They can be prepared using wet chemical methods to yield materials with minimal defects. As a result, there is considerable interest in the development of green energy technology from low-cost QD-based devices. Power conversion efficiencies have substantially increased recently due to the use of defect-tolerant perovskite semiconductors¹ and by delocalizing conducting states using inorganic-passivating ligands.² Theoretical modeling via density functional theory (DFT) has assisted in these efforts, now that computer capabilities have advanced to allow for the study of large inorganic clusters that qualify as quantum dots. DFT has been used to characterize QD surface defects and the microscopic nature of dopants in guest/host systems.^{3–6} Recently, metal-rich “nonstoichiometric” models have been developed, whereby metal halides are used to passivate the surface.^{7–9} They experience minimal surface reconstruction and thus retain a high degree of symmetry; furthermore, the lowest unoccupied molecular orbital (LUMOs) (i.e., conduction states) display particle-in-a-sphere character, which is a long-standing paradigm for QD electronic structure. Finally, these models are justified as many nanomaterials have metal-rich stoichiometries.^{4,10}

This study began during an experimental investigation into the electronic structure of copper-doped InP quantum dots using time-resolved X-ray absorption spectroscopy (TD-

XAS).¹¹ It is well established that copper is oxidized by holes in many semiconductor systems,¹² which was interrogated via direct observation of the dopant’s oxidation state upon photoexcitation using TD-XAS. DFT was meant to provide additional characterization; however, the calculations presented in ref 11 were inconsistent with the experimental results. For example, copper-doped carboxylate-terminated InP models such as $(\text{CH}_3\text{COOH}_2)_{20}\text{CuIn}_{116}\text{P}_{117}$ were found to have triplet ground states, which is incompatible with the doped Cu:InP QDs’ ability to fluoresce.¹³ An amine-terminated cluster, $(\text{NH}_3)_{40}\text{CuIn}_{116}\text{P}_{117}$, was found to be ground-state singlet; however, time-dependent DFT (TD-DFT) and natural bonding orbital (NBO) analyses did not describe the observation of copper oxidation in the excited state. These failures were attributed to a lack of adequate surface passivation in the models as supported by Gary et al., who demonstrated with unprecedented diffraction studies that small InP clusters have large ligand densities.¹⁴

Received: March 30, 2021

Revised: May 4, 2021

Published: May 19, 2021



As reported here, it was found that many of the discrepancies between the theoretical and experimental results of the previous study¹¹ were due to the need for a robust method for optimizing the ground-state geometry of covalent semiconductor InP clusters passivated with organic ligands. However, nonstoichiometric InP QDs display surprisingly complex electronic structures, such as non-Aufbau configurations, as dictated by size, shape, and the choice of metal salts for inorganic passivation. They may have open-shell singlet ground states, which if realized experimentally would have a significant impact on the use of these nanomaterials for green energy generation.

Experimental and Theoretical Methods: DFT. Density functional theory (DFT) modeling of InP and Cu-doped InP semiconductor clusters was performed using the PBE1/PBE,^{15,16} LC-wPBE,¹⁷ and M06-2x hybrid functionals,⁴ with the LANL2DZ basis set and effective core potentials.^{19–21} The high spin states and open-shell singlets were calculated using spin-unrestricted (U) methods. Copper-doped clusters have two units of negative charge to simulate the substitution of In(+3) with Cu(+1), while undoped InP clusters were modeled as neutral. Gaussian'16²² was used for DFT, time-dependent DFT (TD-DFT) as well as natural transition orbital (NTO) analyses of the excited-state densities.²³ Non-Aufbau electronic structure required analyses with biorthogonalized orbitals. The natural bonding orbital (NBO) 6.0 package was used to analyze electron and hole localizations in the ground and excited states as well as the dopant bonding patterns.²⁴ Projected density of states were calculated using GaussSum.²⁵ Visualization was performed using GaussView.²⁶ These calculations were run on UIC's ACER Computing Cluster.

Open-shell singlet states are created starting at the optimized geometry of a high spin system. The electronic structure first mixes the highest occupied molecular orbital (HOMO) and LUMO of the guess state and is subsequently converged using an unrestricted DFT formalism. Generally, the electronic structure retains the same number of unpaired electrons as the high spin state, although spin contamination is always observed. Subsequent geometry optimization recycles the previous state's electronic structure as the initial guess; furthermore, the optimized geometry is similar to the corresponding high spin state that was used initially.

Experimental Section: InP Synthesis. To a three-neck, round-bottom flask was added 116 mg of indium acetate (0.4 mmol) and 137 mg of myristic acid (0.6 mmol) in 10 mL of 1-octadecene. The solution was degassed at 110 °C, briefly heated to 200 °C under nitrogen, and then cooled to 80 °C and degassed again. In an inert-atmosphere glovebox, 50 mg of (TMS)₃P (0.2 mmol, prepared according to ref 27) was added to 1.5 mL of tri-*n*-octylphosphine (97%, Strem Chemical). The heating mantle was removed, and the phosphorus precursor was injected into the round bottom at 80 °C under nitrogen. The solution was heated to 300 °C for 20 min and then returned to room temperature. The samples were estimated to be 2 nm diameter based on the optical band gap (~500 nm).

It was found that processing core QDs and treating their surfaces with various metal salts resulted in minimal impact on their optical properties (see Figure S8A). As a result, processed InP core QDs were etched with a small quantity of ammonium bifluoride (~8 mg) in a solution of 0.137 g of myristic acid in 10 mL of ODE at 60 °C overnight.²⁸ This decreased the size to ~1.7 nm diameter. Next, the sample was processed via precipitation with dry ethanol. One such sample was split into three portions for zinc and indium chloride/oleylamine surface

treatment including an oleylamine control. These portions were characterized optically, as shown in Figure S8B. The impact of metal salt incubation was to increase the sizes of the samples as evident from a lower-energy band gap (~10 nm red shift in the first absorption feature); furthermore, the fluorescence of samples was affected. Three batches of core InP QDs, treated with NH₄HF₂, were prepared for magnetic susceptibility and ³¹P-shifted spectrum method (SSM) nuclear magnetic resonance (NMR) analyses. Two were treated with zinc and indium salts with additional oleylamine in 3 mL of toluene as per Table 1 (see ref 29), while the third was incubated with oleylamine only as a control. Samples were precipitated and stored in a glovebox before analyses.

Table 1. Surface Treatment Parameters for InP QDs Using Metal Salts in Oleylamine

metal salt (mass)	mass QD (mg)	mass oleylamine (mg)
none (control)	45.1	38
InCl ₃ (30 mg)	50.6	38
ZnCl ₂ (18 mg)	50.6	38

Characterization: Magnetic Susceptibility. Data were taken using a Quantum Design MPMSXL Squid magnetometer at the Center for Nanoscale Materials at Argonne National Laboratory. Linearity against the applied field was measured at 300 and 400 °C. The magnetic moment was measured over this temperature range in 20 °C increments.

Solid-State NMR. The QD dispersions were precipitated and loaded into a magic-angle spinning (MAS) spinner for ³¹P analyses. All solid-state NMR experiments were performed on a Bruker Avance III spectrometer equipped with a 400 MHz Oxford wide-bore magnet and a Bruker HXY 1.9 mm MAS triple-resonance probe. Topspin 3.6.2 software on a CentOS 7 Linux system was used to control the experiments. The MAS spinning speed (ν_r) was set to 24 000 ± 1 Hz with an MAS2 spinning module and low-temperature VT using a Bruker Xtreme chiller. The ³¹P NMR signal was referenced to 0 ppm in aqueous 85% H₃PO₄. Single-pulse ³¹P 1D was acquired with a sweep width of 120 kHz, 2048 data points, a 60 s recycle delay, a 100 kHz radiofrequency (RF) field on ³¹P for hard pulses, a 100 kHz 1H TPPM15 decoupling,³⁰ and 1024 scans. 1D ³¹P cross-polarization magic-angle spinning (CP-MAS) was acquired with the same parameters above including a CP transfer contact time of 5 ms having a 50% hyperbolic tangent shape on ³¹P and square pulse spinlock on ¹H at RF fields of 3.5 × ν_r and 2.5 × ν_r on ¹H and ³¹P, respectively. Recycle delays were set to 4 s, and 6000 transients were acquired. 1D ³¹P dipolar insensitive nuclei enhancement by polarization transfer (INEPT)³¹ was also acquired with the same parameters above, except for a recycle delay of 0.1 s, 82 000 transients, and tau set to 27 μ s.

RESULTS AND DISCUSSION

Several models of surface-passivated InP quantum dot-sized clusters were examined using DFT and experimental methods. The purpose was to address the DFT prediction of triplet ground states for (NH₃)₄₀CuIn₁₁₆P₁₁₇ and (CH₃COOH₂)₂₀CuIn₁₁₆P₁₁₇ as reported in ref 11, which is not sensible for a direct band-gap semiconductor regardless of quantum confinement effects. The hypothesis was that the addition of surface ligands would resolve the issue, which was found to be productive as an (NH₃)₆₄CuIn₁₁₆P₁₁₇ model was found to be ground-state singlet and correctly described copper

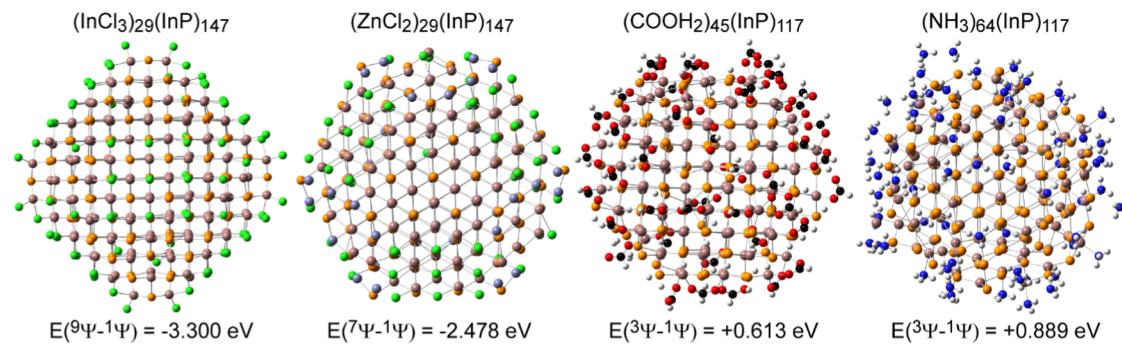


Figure 1. Optimized geometries and energy splittings between paramagnetic and diamagnetic states for InP model systems reveal nonet and septet ground states for the nonstoichiometric $(\text{InCl}_3)_{29}(\text{InP})_{147}$ and $(\text{ZnCl}_2)_{29}(\text{InP})_{147}$ clusters, respectively. Passivation with organic ligands imparts a singlet ground state.

oxidation and modulated bonding to the surrounded matrix in the first excited state.⁹ Concerning carboxylate ligands, a heavily passivated $(\text{H}_3\text{C}_2\text{O}_2)_{51}\text{In}_{37}\text{P}_{20}$ model based on the X-ray diffraction studies of Gary et al. was found to have a singlet ground state (see Figure S1 of the SI).¹⁴ However, the addition of ligands to a larger carboxylate-ligated copper-doped InP cluster, $(\text{HCO}_2\text{H})_{45}\text{CuIn}_{116}\text{P}_{117}$, did not result in a singlet ground state. To explore surface passivation further, inorganically passivated nonstoichiometric systems $(\text{InCl}_3)_{29}\text{CuIn}_{146}\text{P}_{147}$ and $(\text{ZnCl}_2)_{29}\text{CuIn}_{146}\text{P}_{147}$ were developed and found to have paramagnetic ground states.

Alteration of the size and charge of the models did not help, neither did changing the DFT method from PBE1PBE^{15,16} to the more robust LC-wPBE¹⁷ (see Tables S1 and S2 of the SI). Finally, to simplify the underlying electronic structure, neat InP clusters shown in Figure 1 were studied: $(\text{NH}_3)_{64}(\text{InP})_{117}$, $(\text{COOH}_2)_{45}(\text{InP})_{117}$, $(\text{InCl}_3)_{29}(\text{InP})_{147}$, and $(\text{ZnCl}_2)_{29}(\text{InP})_{147}$. Surprisingly, all models aside from the amine were paramagnetic (see Table S3). To ascertain whether these results were artifactual or the result of a physical phenomenon related to QD surface passivation, several models incorporating ligands across the spectrochemical series were created to investigate the effect of surface passivation on the ground states' total spin. The results shown in Figure 2A and Table S4 reveal no systematic trend; at best, the data are nonsensical. At this point, it became clear that there was a problem with the methodology.

Concerning the organic ligand-passivated models, a breakthrough occurred when the geometries were reoptimized at the M06-2x/LANL2DZ level of theory. The Minnesota '06 (M06) family are range-corrected DFT functionals that were developed to incorporate the exact Hartree–Fock exchange energy.¹⁸ These functionals accurately describe a wide variety of molecular properties and can outperform other methods when evaluating singlet–triplet energy gaps.³² Starting with the PBE1PBE-optimized geometry, the energies of all models, aside from the CO-ligated cluster, decreased during reoptimization such that the singlet became the ground state, as shown in Figure 2B. At this point, it was not clear whether the use of a range-corrected functional vs the effort applied toward geometry optimization was responsible for the changeover in the ground state's spin character. To this end, the M06-2x-optimized structures were used as starting points for another round of geometry optimizations at the original PBE1PBE/LANL2DZ level of theory. In every case, the energies dropped significantly compared to the original PBE1PBE-optimized structures, and the trends concerning the spin-state energy gaps were preserved from the more expensive M06-2x calculations, as shown in

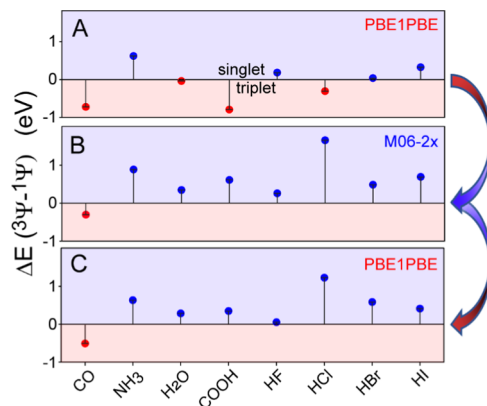


Figure 2. ΔE (triplet–singlet) ground-state energy splitting for various models at the PBE1PBE and M06-2x levels of theory. (A) Ligation of $\text{In}_{117}\text{P}_{117}$ clusters across the spectrochemical series reveals no systematic trend for the ground spin state at the PBE1PBE level of theory. (B, C) Singlet (diamagnetic) ground states are realized following a multistep geometry optimization procedure. These data are summarized in Table S4 in the Supporting Information.

Figure 2B,C. These results demonstrate that all of the original cluster models initially converged to geometries that provided poor descriptions of the material systems. The fact that so many models independently fell into this trap is of concern, a problem that is exacerbated by the large number of degrees of freedom that negate the possibility for ever locating a true global minimum. As a result, it is advised that future DFT investigations of similar covalent semiconductor clusters employ a robust process by which geometry optimizations are perturbed by switching between DFT functionals multiple times. As for the odd case of CO ligation, it was found that carbonyl may coordinate across multiple sites at the InP surface, as shown in Figure S2. As a result, the CO-ligated system was not studied further.

Regardless of the rigor applied to their geometry optimizations, nonstoichiometric $(\text{InCl}_3)_{29}(\text{InP})_{147}$ and $(\text{ZnCl}_2)_{29}(\text{InP})_{147}$ clusters were found to have nonet and septet ground states, respectively (see Table S5). Examination of the density of states (DOS) and spin densities as a function of increasing state multiplicity helps explain these observations. As can be seen in Figure 3, the number of $(\text{InCl}_3)_{29}(\text{InP})_{147}$ HOMO electrons near -7.6 eV decreases as the spin multiplicity increases, which widens the band gap. The spin density plots reveal electrons crowding to the surface of the particle. An identical evolution of the electronic structure was observed in

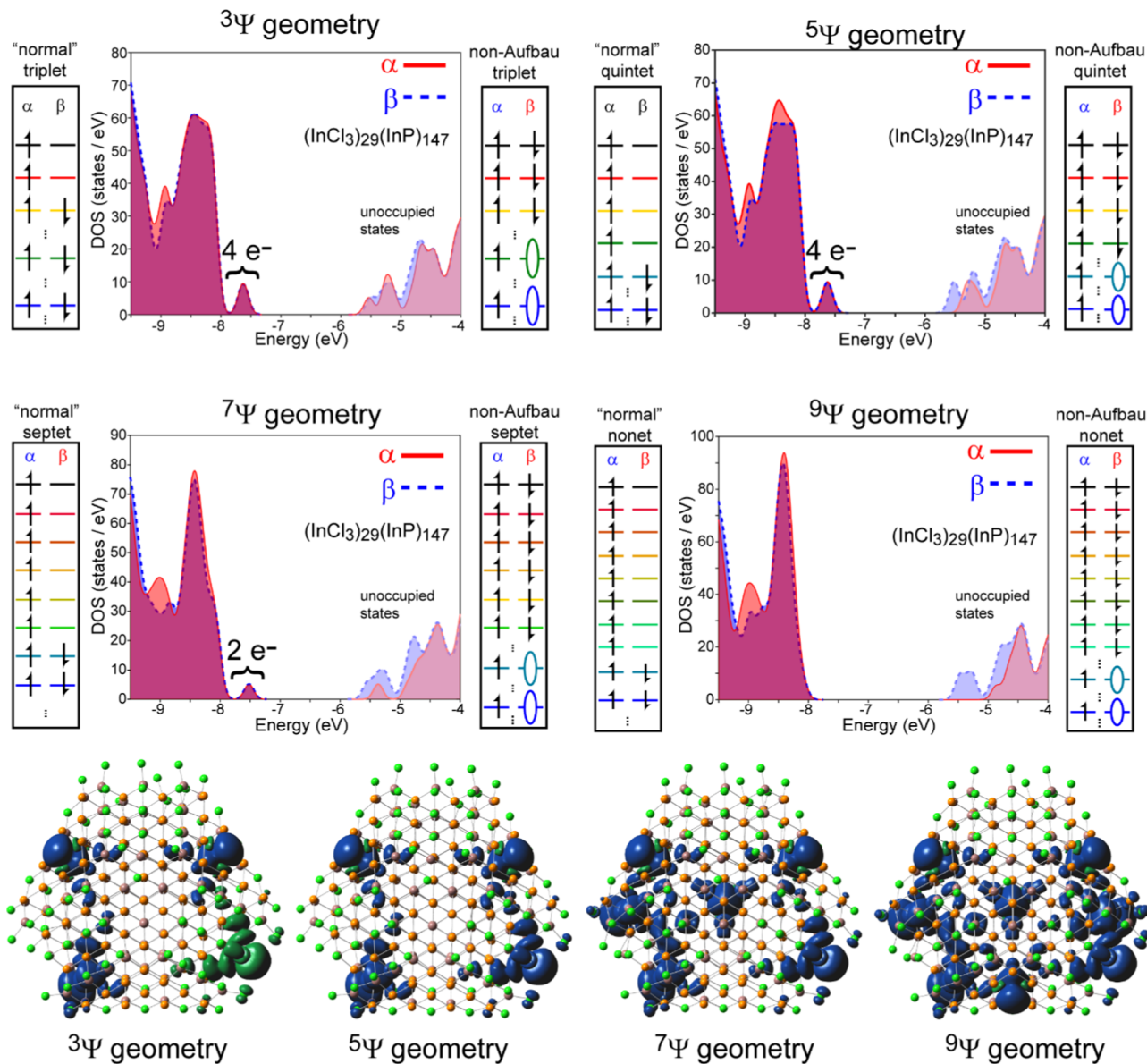


Figure 3. Top: DOS and electronic configuration of high spin states of $(\text{InCl}_3)_{29}(\text{InP})_{147}$. The DOS reveal an opening of the band gap as the multiplicity approaches $S = 9$ (nonet), which is the ground state. The α and β valence orbitals overlap at the band edges, resulting in non-Aufbau configurations. Bottom: spin density plots at the optimized geometries of the various spin states of $(\text{InCl}_3)_{29}(\text{InP})_{147}$ reveal electrons crowding at the surfaces of the clusters.

$(\text{ZnCl}_2)_{29}(\text{InP})_{147}$, as shown in Figure S3 of the SI. These data suggest that the stability of the high multiplicity state is due to electrons occupying metal halide-passivated surface sites that realize lower total energy via minimization of overlap between the unpaired electrons. This hypothesis was tested by examining the size dependence of the ground-state multiplicity. It was found that slightly decreasing the size of the cluster, $(\text{InCl}_3)_{30}(\text{InP})_{140}$, resulted in a ground septate state, while the smallest system, $(\text{InCl}_3)_{13}(\text{InP})_{55}$, is ground-state singlet (see Figure S4). This is attributed to the fact that smaller models must have greater interactions among surface-bound electrons, which prevents the observation of unpaired electrons in the ground state.

It is curious to note that all of the DOS of high spin states shown in Figure 3 have fully overlapping occupied α and β orbitals near the band edge. To understand this observation, it is prudent to first examine the DOS of the organic-ligated CdSe

cluster shown in Figure 4. This system is a ground-state singlet and is thus “well behaved”. There is a -4 eV band gap at the M06-2x/LANL2DZ level of theory, as shown in Figure 4A. To create a triplet excited state, a β -electron is flipped to occupy the LUMO α orbital. This instigates an electronic structural rearrangement that lowers the energy of the newly occupied α -HOMO level away from the valence into the gap, as shown in Figure 4A; note that the α and β manifolds are decoupled in spin-unrestricted DFT calculations. Optimization of the triplet-state geometry causes the energy of the highest occupied α -HOMO state to lower further, as shown in Figure 4B. Similar results were observed in the $(\text{NH}_3)_{64}(\text{InP})_{117}$ cluster that is also ground-state singlet (see Figure S5). The DOS of these high spin states contrast the ground nonet state of $(\text{InCl}_3)_{29}(\text{InP})_{147}$ in Figure 3 due to the fact that the latter’s frontier α and β orbitals overlap. This can only be possible if the imbalance in the number of α and β orbitals is accounted for at lower energy than the band

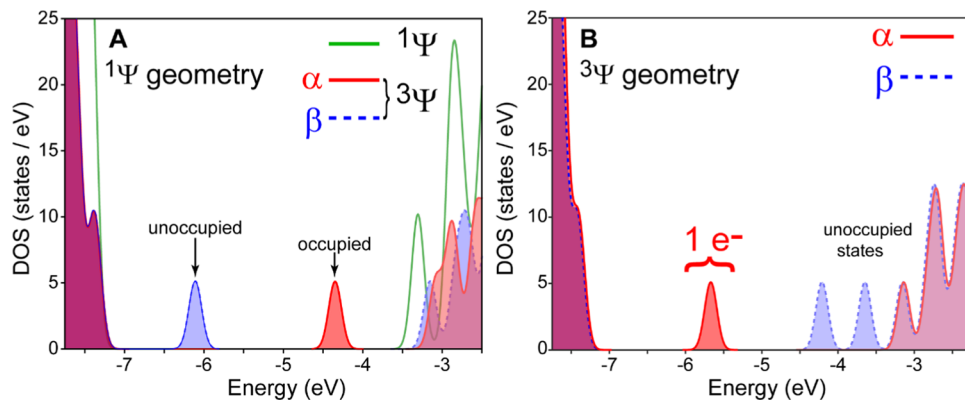


Figure 4. (A) DOS of $(\text{HCO}_2\text{H})_{18}(\text{CdSe})_{114}$ of the singlet (green line) and triplet states (α red, β blue) at the optimized singlet geometry reveal energetic relaxation of the singly occupied α of the triplet away from the conduction band edge. (B) After triplet-state geometry optimization, the highest occupied α electron resides closer to the valence band edge.

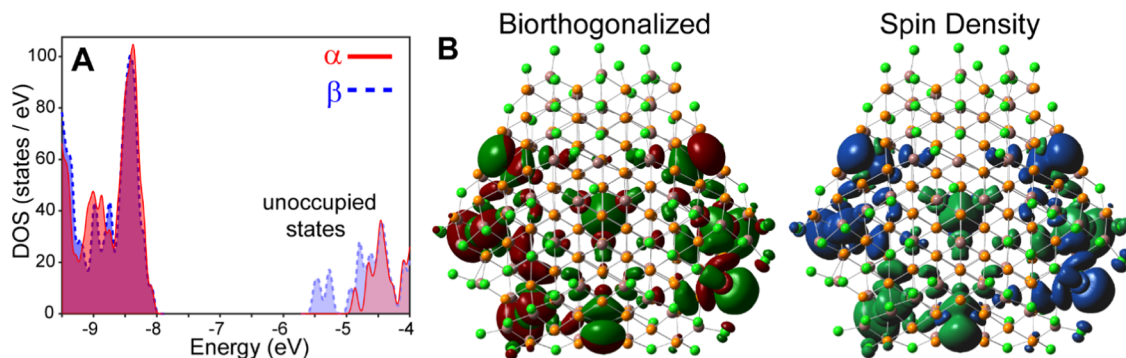


Figure 5. (A) Density of states and (B) biorthogonal orbitals and spin density plots for an open-shell singlet ground state of $(\text{InCl}_3)_{29}(\text{InP})_{147}$ consisting of eight unpaired electrons. The similarity of the DOS and surface-bound probability amplitudes with the near-degenerate nonet state shown in Figure 3 is considerable.

edge. The same was observed in the ground septet state of $(\text{ZnCl}_2)_{29}(\text{InP})_{147}$; furthermore, the projected density of states reveal that the surface-passivating ZnCl_2 orbitals are well below the valence edge, as shown in Figure S6. As a result, the unpaired electrons that impart the total spin are likewise below the valence state. These data reveal that the nonstoichiometric systems have non-Aufbau electronic configurations often found in diradicals.³³ Such an electronic arrangement may seem farcical from the perspective of calculating the total energy as the sum of occupied orbitals' energies. However, to quote ref 33, the Pauli principle requires that "all of the occupied orbitals describe all electrons simultaneously", which introduced such complexity to quantum mechanical calculations that allow for non-Aufbau electron occupancies in the ground state. The most important aspect of this observation is that non-Aufbau configurations afford the possibility that inorganic-passivated InP clusters may have open-shell singlet ground states.

Open-shell singlet ground states have unpaired electrons residing in near-degenerate frontier orbitals of minimal spatial overlap. Examples in the area of organic chemistry include oligoacenes³⁴ and Chichibabin's hydrocarbon,³⁵ which have enhanced nonlinear optical properties and high yields of singlet fission. Organometallic compounds can also have open-shell singlet ground states,^{36,37} usually by partitioning an α and β electron between metal- and ligand-centered electronic states. Both theoretical and experimental characterizations of open-shell singlet species are problematic.³⁸ Theoretically, one cannot apply standard restricted ab initio schemes unless doubly excited

configurations are included, which substantially (and unobtainably for a QD model) increases the computational cost. Unrestricted DFT methods³⁹ are more accurate but suffer from spin contamination.³² Other methods include the EOM-CCD, spin-flip, and the spin-projection technique.^{32,40} In this study, open-shell singlet states converged for both $(\text{InCl}_3)_{29}(\text{InP})_{147}$ and $(\text{ZnCl}_2)_{29}(\text{InP})_{147}$ that were essentially degenerate with the nonet and septet, respectively, as summarized in Table S6. Biorthogonalization of the orbital manifold revealed the same number of unpaired electrons as well. Furthermore, it can be seen in Figure 5 that the spin density and biorthogonalized orbitals of the open-shell singlet are basically identical to those of the paramagnetic $(\text{InCl}_3)_{29}(\text{InP})_{147}$ nonet state. Clearly, the states are localized to the surface, which minimizes the interaction of the electrons with each other. Identical results were obtained with the zinc-passivated cluster (see Figure S7). Such an observation of open-shell singlet quantum dots is exciting due to the potential for enhanced conductive and nonlinear properties that are afforded.

Although the open-shell diamagnetic and paramagnetic states of the nonstoichiometric models were essentially degenerate according to DFT, most likely the open-shell singlet configurations are the lowest energy followed by high spin states. Unfortunately, unrestricted DFT is not suitable for quantifying this splitting between energy levels, and as such, an experimental investigation was instigated. Although open-shell singlets are diamagnetic and thus silent in many magnetic-based spectroscopies (electron paramagnetic resonance (EPR), for

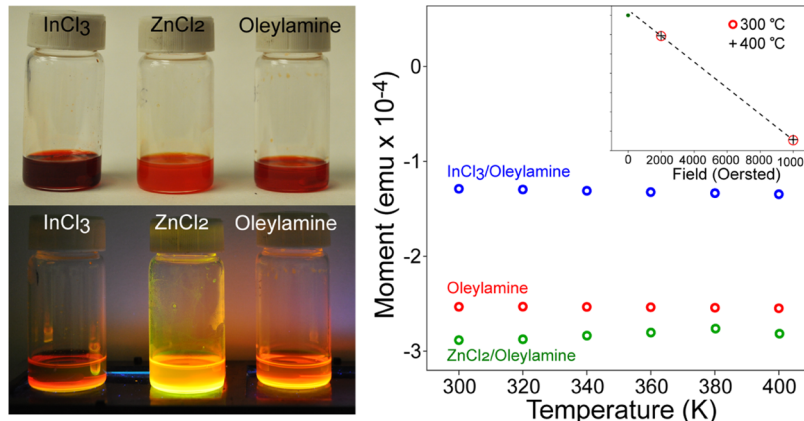


Figure 6. (Left) Room light and fluorescent images of InP QDs incubated with various metal salts to treat the surface states. (Right) Temperature-dependent magnetic susceptibility reveals no alteration of the spin density of samples over 300 → 400 K. Inset: linearity of the susceptibility due to the applied field.

example),⁴¹ the signal from low-lying triplet states may be observed in temperature-dependent studies as evidence of an open-shell singlet ground-state character.⁴² To this end, variable temperature magnetic susceptibility and NMR measurements on surface-modified InP QDs were performed. Samples of InP were synthesized, surface-treated with fluoride, and then incubated with InCl₃ and ZnCl₂ in oleylamine.²⁹ An increase in the fluorescence was observed, as shown in Figures 6 and S6, which is consistent with previous reports of inorganic passivation with metal halide salts.²⁹ Unfortunately, none of the samples exhibited an increase in magnetic susceptibility or NMR resonance broadening over the range of temperatures studied^{42,43} (see Figures 6 and S9). This may be due to the modest temperature ceiling accessible to these experiments (~100 °C) or perhaps that open-shell species can only be realized from clusters with the exact stoichiometries of the models examined herein. To study the latter, the non-stoichiometric DFT models were ligated with NH₃ to provide a more realistic representation of the samples. This resulted in complete quenching of the paramagnetic ground states (see Table S5). The first excited state of (NH₃)_x(ZnCl₂)₂₉(InP)₁₄₇ was found to be triplet, while the (NH₃)_x(InCl₃)₂₉(InP)₁₄₇ cluster had essentially degenerate triplet to nonet first excited states. The energy gaps were found to be substantial, on the order of 1 → 5 eV. This reveals that disrupting the surface states via an electron-donating species returned the systems to “normal” diamagnetic ground states and that observing thermally activated high spin character would require extremely high temperatures.

CONCLUSIONS

The application of model chemistries can augment experimental findings on nanomaterials with microscopic details that are erstwhile inaccessible. Predictions of new phenomena are also possible, as demonstrated here for the potential for highly faceted semiconductor quantum dots passivated with metal halide salts to display open-shell singlet ground states. If proper engineering of QD products can render these predictions true, then many applications in optics and green energy will benefit. It may be necessary to embed the nanomaterials within all inorganic matrices; furthermore, the arrangement of inorganic surfactants can affect the electronic structure via the formation of “displacement” trap states.⁴ This study also demonstrates potential pitfalls concerning the application of model chem-

istries to covalent III–V QDs. Difficulties were encountered due to the electronic structure’s dependence on the geometry. Although expensive, it was found that various model systems could be perturbed outside of local minima by the application of different functionals. Only then were resultant characterizations consistent with previous experimental results.

ASSOCIATED CONTENT

Supporting Information

The Supporting Information is available free of charge at <https://pubs.acs.org/doi/10.1021/acs.jpcc.1c02874>.

Additional computational and experimental data; tabulated data on model InP cluster energies as a function of stoichiometry and method; and also optical data of surface-treated InP QDs as well as temperature-dependent NMR data ([PDF](#))

AUTHOR INFORMATION

Corresponding Author

Preston T. Snee – Department of Chemistry, University of Illinois at Chicago, Chicago, Illinois 60607-7061, United States; orcid.org/0000-0002-6544-6826; Email: sneep@uic.edu

Complete contact information is available at: <https://pubs.acs.org/10.1021/acs.jpcc.1c02874>

Notes

The author declares no competing financial interest.

ACKNOWLEDGMENTS

This work was supported by the University of Illinois at Chicago. The author acknowledges the Donors of the American Chemical Society Petroleum Research Fund for partial support of this research, Daniel J. McElheny for solid-state NMR measurements, Brandon Fisher and Marcell Pálmai for assistance with temperature-dependent magnetic susceptibility measurements, Ivan Infante with discussion and assistance with nonstoichiometric models of quantum dots, and the Advanced Cyberinfrastructure for Education and Research (ACER) group at the University of Illinois at Chicago for providing computational resources and services for research results delivered within this paper. URL: <https://acer.uic.edu>. The use of the Center for Nanoscale Materials, an Office of Science user facility, was

supported by the U.S. Department of Energy, Office of Science, Office of Basic Energy Sciences, under Contract No. DE-AC02-06CH11357.

■ REFERENCES

- (1) Protesescu, L.; Yakunin, S.; Bodnarchuk, M. I.; Krieg, F.; Caputo, R.; Hendon, C. H.; Yang, R. X.; Walsh, A.; Kovalenko, M. V. Nanocrystals of Cesium Lead Halide Perovskites (CsPbX_3 , X = Cl, Br, and I): Novel Optoelectronic Materials Showing Bright Emission with Wide Color Gamut. *Nano Lett.* **2015**, *15*, 3692–3696.
- (2) Dolzhnikov, D. S.; Zhang, H.; Jang, J.; Son, J. S.; Panthani, M. G.; Shibata, T.; Chattopadhyay, S.; Talapin, D. V. Composition-Matched Molecular “Solders” for Semiconductors. *Science* **2015**, *347*, 425–428.
- (3) Voznyy, O.; Thon, S. M.; Ip, A. H.; Sargent, E. H. Dynamic Trap Formation and Elimination in Colloidal Quantum Dots. *J. Phys. Chem. Lett.* **2013**, *4*, 987–992.
- (4) Giansante, C.; Infante, I. Surface Traps in Colloidal Quantum Dots: A Combined Experimental and Theoretical Perspective. *J. Phys. Chem. Lett.* **2017**, *8*, 5209–5215.
- (5) Hassan, A.; Zhang, X.; Liu, X.; Rowland, C. E.; Jawaid, A. M.; Chattopadhyay, S.; Gulec, A.; Shamirian, A.; Zuo, X.; Klie, R. F.; et al. Charge Carriers Modulate the Bonding of Semiconductor Nanoparticle Dopants As Revealed by Time-Resolved X-Ray Spectroscopy. *ACS Nano* **2017**, *11*, 10070–10076.
- (6) Nelson, H. D.; Li, X. S.; Gamelin, D. R. Computational Studies of the Electronic Structures of Copper-Doped CdSe Nanocrystals: Oxidation States, Jahn-Teller Distortions, Vibronic Bandshapes, and Singlet-Triplet Splittings. *J. Phys. Chem. C* **2016**, *120*, 5714–5723.
- (7) Voznyy, O. Mobile Surface Traps in CdSe Nanocrystals with Carboxylic Acid Ligands. *J. Phys. Chem. C* **2011**, *115*, 15927–15932.
- (8) Voznyy, O.; Zhitomirsky, D.; Stadler, P.; Ning, Z.; Hoogland, S.; Sargent, E. H. A Charge-Orbital Balance Picture of Doping in Colloidal Quantum Dot Solids. *ACS Nano* **2012**, *6*, 8448–8455.
- (9) Snee, P. T. Semiconductor Quantum Dot FRET: Untangling Energy Transfer Mechanisms in Bioanalytical Assays. *TrAC, Trends Anal. Chem.* **2020**, *123*, No. 115750.
- (10) Stein, J. L.; Mader, E. A.; Cossairt, B. M. Luminescent InP Quantum Dots with Tunable Emission by Post-Synthetic Modification with Lewis Acids. *J. Phys. Chem. Lett.* **2016**, *7*, 1315–1320.
- (11) Hassan, A.; Zhang, X. Y.; Liu, C. M.; Snee, P. T. Electronic Structure and Dynamics of Copper-Doped Indium Phosphide Nanocrystals Studied with Time-Resolved X-Ray Absorption and Large-Scale DFT Calculations. *J. Phys. Chem. C* **2018**, *122*, 11145–11151.
- (12) Knowles, K. E.; Hartstein, K. H.; Kilburn, T. B.; Marchioro, A.; Nelson, H. D.; Whitham, P. J.; Gamelin, D. R. Luminescent Colloidal Semiconductor Nanocrystals Containing Copper: Synthesis, Photo-physics, and Applications. *Chem. Rev.* **2016**, *116*, 10820–10851.
- (13) Xie, R.; Peng, X. Synthesis of Cu-Doped InP Nanocrystals (d-Dots) with ZnSe Diffusion Barrier as Efficient and Color-Tunable NIR Emitters. *J. Am. Chem. Soc.* **2009**, *131*, 10645–10651.
- (14) Gary, D. C.; Flowers, S. E.; Kaminsky, W.; Petrone, A.; Li, X.; Cossairt, B. M. Single-Crystal and Electronic Structure of a 1.3 nm Indium Phosphide Nanocluster. *J. Am. Chem. Soc.* **2016**, *138*, 1510–1513.
- (15) Perdew, J. P.; Burke, K.; Ernzerhof, M. Generalized Gradient Approximation Made Simple. *Phys. Rev. Lett.* **1996**, *77*, 3865–3868.
- (16) Adamo, C.; Barone, V. Toward Reliable Density Functional Methods without Adjustable Parameters: The PBE0 Model. *J. Chem. Phys.* **1999**, *110*, 6158–6170.
- (17) Vydrov, O. A.; Scuseria, G. E. Assessment of a Long-Range Corrected Hybrid Functional. *J. Chem. Phys.* **2006**, *125*, No. 234109.
- (18) Zhao, Y.; Truhlar, D. G. The M06 Suite of Density Functionals for Main Group Thermochemistry, Thermochemical Kinetics, Non-covalent Interactions, Excited States, and Transition Elements: Two New Functionals and Systematic Testing of Four M06-Class Functionals and 12 Other Functionals. *Theor. Chem. Acc.* **2008**, *120*, 215–241.
- (19) Hay, P. J.; Wadt, W. R. Ab Initio Effective Core Potentials for Molecular Calculations - Potentials for The Transition-Metal Atoms Sc To Hg. *J. Chem. Phys.* **1985**, *82*, 270–283.
- (20) Hay, P. J.; Wadt, W. R. Ab Initio Effective Core Potentials for Molecular Calculations - Potentials For K To Au Including The Outermost Core Orbitals. *J. Chem. Phys.* **1985**, *82*, 299–310.
- (21) Wadt, W. R.; Hay, P. J. Ab Initio Effective Core Potentials for Molecular Calculations - Potentials For Main Group Elements Na To Bi. *J. Chem. Phys.* **1985**, *82*, 284–298.
- (22) Frisch, M. J.; Trucks, G. W.; Schlegel, H. B.; Scuseria, G. E.; Robb, M. A.; Cheeseman, J. R.; Scalmani, G.; Barone, V.; Petersson, G. A.; Nakatsuji, H. et al. *Gaussian 16*, revision C.01; Gaussian, Inc.: Wallingford, CT, 2016.
- (23) Martin, R. L. Natural Transition Orbitals. *J. Chem. Phys.* **2003**, *118*, 4775–4777.
- (24) Glendening, E. D.; Badenhoop, J. K.; Reed, A. E.; Carpenter, J. E.; Bohmann, J. A.; Morales, C. M.; Landis, C. R.; Weinhold, F. NBO 6.0; Theoretical Chemistry Institute, University of Wisconsin: Madison, 2013.
- (25) O’Boyle, N. M.; Tenderholt, A. L.; Langner, K. M. Cclib: A Library for Package-Independent Computational Chemistry Algorithms. *J. Comput. Chem.* **2008**, *29*, 839–845.
- (26) Dennington, R.; Keith, T.; Millam, J. *GaussView*; Semichem Inc.: Shawnee Mission, KS, 2009.
- (27) Holz, J.; Zayas, O.; Jiao, H.; Baumann, W.; Spannenberg, A.; Monsees, A.; Riermeier, T. H.; Almena, J.; Kadyrov, R.; Börner, A. A Highly Tunable Family of Chiral Bisphospholanes for Rh-Catalyzed Enantioselective Hydrogenation Reactions. *Chem. - Eur. J.* **2006**, *12*, 5001–5013.
- (28) Chandrasiri, H. B.; Kim, E. B.; Snee, P. T. Sterically Encumbered Tris(trialkylsilyl) Phosphine Precursors for Quantum Dot Synthesis. *Inorg. Chem.* **2020**, *59*, 15928–15935.
- (29) Kirkwood, N.; Monchen, J. O. V.; Crisp, R. W.; Grimaldi, G.; Bergstein, H. A. C.; du Fossé, I.; van der Stam, W.; Infante, I.; Houtepen, A. J. Finding and Fixing Traps in II–VI and III–V Colloidal Quantum Dots: The Importance of Z-Type Ligand Passivation. *J. Am. Chem. Soc.* **2018**, *140*, 15712–15723.
- (30) Bennett, A. E.; Rienstra, C. M.; Auger, M.; Lakshmi, K. V.; Griffin, R. G. Heteronuclear Decoupling in Rotating Solids. *J. Chem. Phys.* **1995**, *103*, 6951–6958.
- (31) Wickramasinghe, N. P.; Ishii, Y. Sensitivity Enhancement, Assignment, and Distance Measurement in ^{13}C Solid-State NMR Spectroscopy for Paramagnetic Systems under Fast Magic Angle Spinning. *J. Magn. Reson.* **2006**, *181*, 233–243.
- (32) Ess, D. H.; Cook, T. C. Unrestricted Prescriptions for Open-Shell Singlet Diradicals: Using Economical Ab Initio and Density Functional Theory to Calculate Singlet-Triplet Gaps and Bond Dissociation Curves. *J. Phys. Chem. A* **2012**, *116*, 4922–4929.
- (33) Gryn’ova, G.; Coote, M. L.; Corminboeuf, C. Theory and Practice of Uncommon Molecular Electronic Configurations. *Wiley Interdiscip. Rev.: Comput. Mol. Sci.* **2015**, *5*, 440–459.
- (34) Bendikov, M.; Duong, H. M.; Starkey, K.; Houk, K. N.; Carter, E. A.; Wudl, F. Oligoacenes: Theoretical Prediction of Open-Shell Singlet Diradical Ground States. *J. Am. Chem. Soc.* **2004**, *126*, 7416–7417.
- (35) Tschitschibabin, A. E. Über Einige Phenylerte Derivate Des p, p-Ditolyls. *Ber. Dtsch. Chem. Ges.* **1907**, *40*, 1810–1819.
- (36) Abram, S.-L.; Monte-Pérez, I.; Pfaff, F. F.; Farquhar, E. R.; Ray, K. Evidence of Two-State Reactivity in Alkane Hydroxylation by Lewis-Acid Bound Copper–Nitrile Complexes. *Chem. Commun.* **2014**, *50*, 9852–9854.
- (37) Thompson, N. B.; Oyala, P. H.; Dong, H. T.; Chalkley, M. J.; Zhao, J.; Alp, E. E.; Hu, M.; Lehnert, N.; Peters, J. C. Electronic Structures of an $[\text{Fe}(\text{NNR}_2)]^+/\text{O}/-$ Redox Series: Ligand Non-innocence and Implications for Catalytic Nitrogen Fixation. *Inorg. Chem.* **2019**, *58*, 3535–3549.
- (38) Slipchenko, L. V. Electronic Structure Calculations of Open-Shell Molecules. Ph.D. Thesis, University of Southern California: Los Angeles, CA, 2005.

(39) Gräfenstein, J.; Kraka, E.; Cremer, D. Density Functional Theory for Open-Shell Singlet Biradicals. *Chem. Phys. Lett.* **1998**, *288*, 593–602.

(40) Krylov, A. I. The Quantum Chemistry of Open-Shell Species. In *Reviews in Computational Chemistry*; John Wiley & Sons Ltd., 2017; pp 151–224.

(41) Mondal, K. C.; Roy, S.; Roesky, H. W. Silicon Based Radicals, Radical Ions, Diradicals and Diradicaloids. *Chem. Soc. Rev.* **2016**, *45*, 1080–1111.

(42) Li, Y.; Heng, W.-K.; Lee, B. S.; Aratani, N.; Zafra, J. L.; Bao, N.; Lee, R.; Sung, Y. M.; Sun, Z.; Huang, K.-W.; et al. Kinetically Blocked Stable Heptazethrene and Octazethrene: Closed-Shell or Open-Shell in the Ground State? *J. Am. Chem. Soc.* **2012**, *134*, 14913–14922.

(43) Das, S.; Herng, T. S.; Zafra, J. L.; Burrezo, P.; Kitano, M.; Ishida, M.; Gopalakrishna, T.; Hu, P.; Osuka, A.; Casado, J.; et al. Fully Fused Quinoidal/Aromatic Carbazole Macrocycles with Poly-Radical Characters. *J. Am. Chem. Soc.* **2016**, *138*, 7782–7790.